Research Square

Preprints are preliminary reports that have not undergone peer review.
They should not be considered conclusive, used to inform clinical practice,
or referenced by the media as validated information.

An Open-Source Platform for Multimodal Electrical and Optical Mapping of Ex Vivo Hearts

Vinicius Silva
Universidade Federal do ABC
Jimena Siles
Universidade Federal do ABC
Tainan Neves
Universidade Federal do ABC
Angélica Quadros
Universidade Federal do ABC
Murilo Leal
Universidade Federal do ABC
José Gomes
Universidade Federal do ABC
Shiva Eghdamian
Universidade Federal do ABC
Ilija Uzelac
Virginia Commonwealth University
João Salinet
joao.salinet@ufabc.edu.br

Universidade Federal do ABC

Article

Keywords:

Posted Date: September 17th, 2026

DOI: https://doi.org/10.21203/rs.3.rs-10910308/v1

License: This work is licensed under a Creative Commons Attribution 4.0 International License.
Read Full License

Additional Declarations: No competing interests reported.

An Open-Source Platform for Multimodal Electrical and Optical Mapping of Ex Vivo Hearts

Vinicius Silva[1], Jimena Siles[1], Tainan Neves[1], Angélica Quadros[1], Murilo Leal[1], José Gomes[1], Shiva Eghdamian[1], Ilija Uzelac[2], and João Salinet [1,*]

[1]HEartLab, Federal University of ABC, São Bernardo do Campo, SP, Brazil
[2]Virginia Commonwealth University, Richmond, VA, United States
[*]joao.salinet@ufabc.edu.br

ABSTRACT

Complex cardiac arrhythmias exhibit dynamic and spatially heterogeneous activation patterns that are difficult to characterize using individual mapping modalities. Experimental platforms that enable synchronized acquisition of complementary electrophysiological measurements across cardiac preparations could facilitate mechanistic studies and quantitative evaluation of cardiac mapping methods. Here, we present an open-source platform for synchronized multimodal mapping of ex vivo perfused hearts, integrating optical mapping, contact-electrical mapping, torso-tank recordings, pacing and arrhythmia induction, physiological monitoring, three-dimensional morphology reconstruction, and centralized experimental control. The platform was implemented in three configurations tailored to different experimental requirements: small-heart whole-organ, large-heart whole-organ, and large-heart epicardial–endocardial mapping. Its operation was demonstrated in rabbit, porcine, and human cardiac preparations, with synchronized recordings obtained during sinus rhythm, ventricular tachycardia, fibrillation, and controlled pacing. A common hardware timing reference and experimental-control interface enabled coordination of independent acquisition systems, physiological measurements, stimulation protocols, metadata, and event logging. The resulting framework provides simultaneous high-resolution optical measurements and electrophysiologically relevant electrical recordings from the same cardiac events, enabling direct investigation of their correspondence across spatial scales and preparation geometries. By combining complementary mapping approaches within a reproducible and adaptable framework, and making the software, firmware, electronic designs, and mechanical files openly available `https://github.com/HEartLab-ufabc/HEartLab-Multimodal-Mapping.git`, this platform provides a foundation for studying complex arrhythmia mechanisms and developing and evaluating cardiac mapping methods relevant to electrophysiological diagnosis and catheter ablation.

Introduction

Cardiac arrhythmias arise from abnormalities in electrical impulse generation and propagation and from their interaction with structural and functional heterogeneity of the myocardium[1]. For complex arrhythmias, including atrial fibrillation (AF), scar-related atrial tachycardia (AT), and ventricular tachycardia (VT), identifying the mechanisms that initiate and sustain abnormal activation is central to both mechanistic research and therapy. Catheter ablation has become an important treatment for these conditions and relies on electroanatomic mapping (EAM) systems to identify abnormal substrate, reconstruct activation sequences, and guide the delivery of ablation lesions. Contemporary systems such as CARTO, EnSite, and Rhythmia combine catheter localization with three-dimensional cardiac geometry and large numbers of intracardiac electrograms to generate activation, voltage, and other electrophysiological maps[2,3]. These electrograms provide direct measurements of extracellular electrical activity with high temporal resolution, but their amplitude, morphology, and timing depend on factors including electrode dimensions and orientation, tissue contact, wavefront direction, reference configuration, and electrical activity arising from surrounding myocardium[4,5]. Consequently, relating individual electrogram features to the underlying pattern of myocardial propagation can become challenging during complex arrhythmias in which multiple or changing wavefronts contribute to the recorded signals.

Despite these technological advances, mapping and ablation of complex arrhythmias remain challenging, particularly when the arrhythmogenic substrate is spatially heterogeneous or when activation changes dynamically during the procedure[3]. Recent clinical trials reported AF recurrence in approximately 30–40% of patients after a first ablation procedure, with some patients requiring repeat interventions[6,7]. These limitations reinforce the need for experimental approaches that can clarify how the electrical signals used for clinical mapping relate to the underlying patterns of myocardial activation.

Controlled experimental models provide an opportunity to make this comparison under well-defined conditions. Optical mapping is particularly valuable in this context because voltage-sensitive dyes allow transmembrane-potential changes to be

recorded at high spatial and temporal resolution, enabling visualization of wavefront propagation, conduction block, focal activation, re-entry, and fibrillatory activity over the exposed myocardial surface[8,9]. This makes optical mapping a powerful reference for studying arrhythmia mechanisms that may be difficult to resolve using electrode recordings alone. At the same time, optical signals and extracellular electrograms represent different electrophysiological quantities, making their simultaneous acquisition particularly useful for investigating how high-resolution myocardial activation is represented in clinically relevant electrical measurements.

A limitation of optical mapping is that it requires direct visual access to the tissue and is therefore used primarily in experimental preparations. This requirement has also motivated approaches that provide access to more than one myocardial surface. In epicardial–endocardial (epi-endo) mapping, opposing surfaces of the myocardial wall are recorded during the same cardiac event, allowing differences in activation and repolarization across the wall to be examined directly[10,11]. Combining epi-endo optical mapping with contact-electrical recordings extends this approach by relating high-resolution activation patterns on both surfaces to the extracellular signals obtained from the same regions.

Several experimental systems have combined optical and electrical recordings to investigate the relationship between myocardial activation and extracellular measurements. Knisley and Neuman used a transparent electrode array to acquire co-localized optical transmembrane-voltage and extracellular-potential measurements from rabbit hearts, demonstrating that activation times obtained from the two modalities can differ according to wavefront direction and the effective interrogation depth of each technique[12]. Chowdhury et al. later combined optical mapping with multi-electrode recordings in cardiac cell cultures and human myocardial slices, extending simultaneous optical–electrical measurements to preparations with different spatial scales and structural complexity[13]. Conformal electronic approaches have also been developed for whole-heart measurements. Xu et al. introduced a three-dimensional elastic membrane shaped to the rabbit epicardium that incorporated electrical electrodes, stimulation sites, and other physiological sensors while remaining sufficiently transparent for simultaneous optical mapping[14]. These studies illustrate different strategies for obtaining complementary optical and electrical measurements from the same cardiac event.

A parallel development has been the expansion of optical mapping from localized fields of view to larger portions of the cardiac surface. Lee et al. developed panoramic optical-mapping systems for Langendorff-perfused rabbit and porcine hearts, demonstrating that multi-camera imaging can capture complex activation patterns over substantially larger regions of the epicardium[15]. The RHYTHM toolkit subsequently provided an open-source implementation combining panoramic optical acquisition, three-dimensional reconstruction, and analysis tools and demonstrated the approach in mouse, rat, and rabbit hearts[16]. More tightly integrated optical–electrical systems have also been developed. The panoramic opto-electrical measurement and stimulation (POEMS) system combined 294 optical fibres and 64 electrodes within a conformal cup surrounding the ventricular surface of mouse hearts, enabling simultaneous panoramic optical and electrical mapping together with localized stimulation[17]. These systems substantially increased either spatial coverage or integration between modalities, although their physical implementations were generally optimized for a particular preparation geometry or experimental objective.

Complementary electrical measurements can also be obtained remotely from the myocardium using body-surface potential mapping (BSPM) and electrocardiographic imaging (ECGi). These approaches seek to characterize cardiac electrical activity from potentials measured outside the heart, but the recorded field is spatially smoothed and attenuated by volume conduction[18]. Torso-tank models provide a controlled experimental environment in which these remotely measured potentials can be compared directly with cardiac-surface measurements. In a porcine model, Bear et al. suspended Langendorff-perfused hearts within a human-shaped torso tank and simultaneously recorded optical action potentials, epicardial electrograms from a 108-electrode sock, and potentials from electrodes distributed over the tank surface[19]. The platform was developed specifically for ECGi validation and allowed reconstructed epicardial activation and repolarization patterns to be compared with both optical and contact-electrical reference measurements. Related porcine torso-tank studies have used simultaneous epicardial and torso recordings to assess the ability of ECGi to identify electrical dyssynchrony and pacing-related activation patterns[20].

Our previous work extended this concept by combining panoramic optical mapping, epicardial multi-electrode arrays, torso-tank recordings, and three-dimensional reconstruction within a single small-heart preparation[21]. In Langendorff-perfused rabbit hearts, synchronized measurements were obtained during sinus rhythm and atrial and ventricular arrhythmias, allowing activation, frequency, and phase characteristics to be evaluated across optical, contact-electrical, torso-tank, and ECGi representations. Agreement between modalities depended on the rhythm and analysis being considered, reinforcing the need for complementary measurements when evaluating complex cardiac activation rather than treating individual mapping modalities as interchangeable representations of the same electrophysiological process.

The epi-endo approach is particularly relevant because cardiac activation occurs through a three-dimensional myocardial wall, and epicardial recordings alone cannot fully describe activity occurring on the endocardial surface or across the wall. Simultaneous epicardial and endocardial measurements allow differences between opposing surfaces to be examined directly without relying on sequential recordings or inferring one surface from the other[10,11]. This provides information complemen-

tary to whole-organ panoramic mapping: whole-heart preparations preserve global cardiac geometry and permit torso-tank measurements, whereas epi-endo preparations provide more direct access to activation on both sides of the ventricular wall.

These experimental requirements become more difficult to combine when moving between preparation sizes. Small isolated hearts are well suited to panoramic imaging, dense contact measurements, and torso-tank experiments, whereas porcine and human hearts require greater perfusion capacity, different mechanical support, larger optical fields of view, and electrical interfaces adapted to their dimensions. Epi-endo experiments impose a different requirement again because both myocardial surfaces must remain accessible to optical and contact-electrical measurements. A platform intended to support these studies must therefore accommodate different preparation geometries while maintaining synchronization between mapping modalities, stimulation, physiological measurements, and experimental records.

Here, we present the first worldwide an open-source experimental platform for synchronized panoramic optical and electrical mapping of ex vivo perfused hearts across these experimental conditions. The platform was implemented in three configurations: small-heart whole-organ mapping, combining panoramic optical, epicardial contact-electrical, and torso-tank measurements; large-heart whole-organ mapping, combining optical and torso-tank recordings in intact porcine and human hearts; and large-heart epi-endo mapping, providing simultaneous optical and contact-electrical access to opposing ventricular surfaces. A common framework for experimental control, physiological monitoring, pacing and arrhythmia induction, synchronization, and data logging was retained across configurations. The platform is available at `https://github.com/HEartLab-ufabc/HEartLab-Multimodal-Mapping.git`, intend to provide a reproducible experimental basis for studying complex arrhythmia mechanisms and for examining how myocardial activation is represented by electrical mapping techniques relevant to arrhythmia diagnosis and ablation.

Results

The platform was implemented across a range of preparation sizes and experimental geometries. The small-heart configuration was validated in 41 experimental sessions using rabbit hearts, whereas the large-heart configurations were applied in 11 human-heart and 8 porcine-heart experiments. Across these preparations, optical and electrical acquisition shared a common hardware timing reference, allowing measurements from the different modalities to be compared during the same cardiac events.

The three configurations addressed different recording requirements. Small hearts allowed simultaneous panoramic optical mapping, local epicardial electrical mapping, and measurement of the surrounding tank-torso electrical field. Large whole hearts provided optical and tank-torso electrical measurements while preserving intact organ geometry. The epi-endo configuration provided direct optical and electrical access to opposing surfaces of the ventricular wall.

Multimodal mapping in small hearts

The small-heart configuration enabled simultaneous optical, contact-electrical, and torso-tank recordings from the same perfused preparation. The recording geometry, tank and MEA dimensions, experimental setup, and representative images acquired by the three cameras are shown in Fig. 1A,B. The three optical views provided complementary coverage of the cardiac surface while the MEAs and tank electrodes recorded local and remote electrical activity during the same acquisition.

Representative right-atrial local activation time (LAT) maps during sinus rhythm are shown in Fig. 1C. Optical activation was evaluated over the region directly covered by the atrial MEA, allowing both measurements to be compared within the same anatomical area. The optical map showed a continuous progression of activation across the tissue, whereas the electrical map reproduced the activation sequence from the discrete electrode measurements after spatial interpolation. Both modalities identified an organized progression from earlier to later activation across the mapped region.

The ability to obtain corresponding maps was retained during arrhythmia. Figure 1D shows optical and contact-electrical LAT maps during VT. Despite the different spatial sampling of the two modalities, regions of earlier and later activation could be identified in both measurements during the same arrhythmic episode.

The surrounding tank electrodes recorded tank-torso activity simultaneously with the optical and MEA signals. Figure 1E shows the corresponding tank timing distribution during ventricular tachycardia. Unlike optical and MEA LATs, which represent activation at or near the myocardial surface, the tank measurements represent the cardiac electrical field after propagation through the conductive tank solution.

Together, these recordings demonstrate three levels of measurement within a single experiment: high-density optical activation over the myocardial surface, local extracellular activity from contact electrodes, and the resulting tank-torso field measured at the tank boundary. This configuration therefore provides paired measurements that can subsequently be used to evaluate how features of local cardiac activation are represented in more distant electrical recordings.

Whole-heart multimodal mapping in large hearts

The large-heart whole-organ configuration extended synchronized optical and tank-torso mapping to intact porcine and human hearts. Figure 2A shows the recording geometry and transparent electrode interfaces, whereas Fig. 2B shows the platform during an experiment with an ex vivo human heart.

Optical fluorescence and tank potentials were recorded simultaneously from opposing regions of the preparation. The transparent electrode PCBs allowed electrical measurements to be obtained from both sides of the tank while maintaining optical access to the heart. The resulting recordings therefore preserved the relationship between direct optical measurements of myocardial activation and electrical potentials measured in the surrounding conductive volume.

Representative maps obtained from the same human heart and pacing site at cycle lengths of 350 and 500 ms are shown in Fig. 2C. Optical LAT maps are presented together with the corresponding tank-torso timing maps recorded from the two opposing PCB interfaces. Because each recording was referenced independently in time, absolute activation times cannot be compared directly between the two pacing conditions.

The optical maps nevertheless show the spatial activation sequence across the imaged region for each pacing cycle length. Both recordings show activation progressing across the field of view from the upper-right region toward the lower-left region, although the spatial distribution of activation times differs between the two conditions. The two tank-electrode interfaces recorded corresponding changes in the tank-torso timing distributions. No quantitative comparison between pacing conditions was performed; these data therefore demonstrate synchronized multimodal acquisition at different pacing rates rather than a rate-dependent change in conduction. A representative synchronized optical and electrical recording from a porcine whole-heart experiment is provided in Supplementary Video S1.

These experiments demonstrate that the multimodal acquisition strategy could be transferred from small hearts to intact preparations with dimensions closer to the human heart while preserving simultaneous optical and tank-torso measurements. Importantly, this was demonstrated directly in human as well as porcine hearts rather than inferred from geometric scaling alone.

Epi-endo mapping in large hearts

The large-heart epi-endo configuration was used when simultaneous access to the epicardial and endocardial surfaces was required. The preparation geometry and experimental chamber are shown in Fig. 3A,B. Optical and contact-electrical activity could be recorded from both surfaces during the same cardiac event.

Representative LAT maps during sinus rhythm are shown in Fig. 3C. Endocardial maps are presented in the left column and epicardial maps in the right column, with optical measurements above the corresponding MEA-derived maps. Both surfaces showed organized propagation during sinus rhythm, and the optical and contact-electrical measurements provided corresponding representations of the activation sequence within their respective mapped regions.

Simultaneous access to both surfaces also allowed more complex rhythms to be examined. Figure 3D shows optical and contact-electrical activation maps during fibrillation. Compared with sinus rhythm, the activation patterns were less spatially organized and showed greater variation across the epicardial and endocardial surfaces. Both optical and electrical measurements captured these changes during the same fibrillatory episode.

The paired recordings are particularly useful because epicardial and endocardial activation were measured directly rather than sequentially or inferred from the opposite surface. This allows differences between the two surfaces to be evaluated without introducing beat-to-beat variation between separate recordings. The configuration therefore complements whole-heart experiments by sacrificing intact organ geometry in exchange for direct epi-endo access.

Three-dimensional reconstruction

Three-dimensional reconstruction was performed after selected whole-heart experiments to recover an experiment-specific representation of the external cardiac geometry. The reconstruction workflow is shown in Fig. 4, including ChArUco-based camera calibration, controlled rotational imaging, silhouette segmentation and correction, and generation of the final surface mesh.

During rotational imaging, multiple views of the preparation were acquired over 360°. The cardiac outline was segmented at each angular position and transformed into the calibrated three-dimensional coordinate system. Combining the silhouettes constrained the volume occupied by the preparation and produced an initial three-dimensional representation.

Geometric correction reduced errors produced by camera alignment and rotational offsets before mesh generation. The reconstructed volume was then converted into a triangulated surface and refined to remove isolated regions, segmentation irregularities, and artefacts introduced by the supporting structures.

The resulting meshes reproduced the main external contours of the preparations and provided a geometry that could be associated with the corresponding experimental recordings. This creates a common anatomical surface for subsequent localization of visible landmarks, electrode positions, and optical fields of view.

The reconstruction is limited to structures represented in the external silhouettes. Internal anatomy and concavities that remained hidden throughout the rotational sequence could not be recovered. The resulting mesh should therefore be interpreted as an experiment-specific external surface rather than a complete anatomical reconstruction.

Discussion

This study presents an open-source platform for synchronized multimodal investigation of ex vivo perfused hearts across different preparation sizes and recording geometries. The platform was validated in rabbit, porcine, and human hearts using three complementary configurations: small-heart whole-organ, large-heart whole-organ, and large-heart epi-endo. Rather than reproducing the same recording arrangement at different scales, each configuration was designed to address a different experimental requirement while retaining common functions for perfusion, physiological monitoring, pacing and arrhythmia induction, synchronization, experimental control, and data recording.

The main motivation for combining these measurements is that no single mapping modality provides a complete description of complex cardiac activation. Optical mapping offers high spatial resolution and allows wavefront propagation to be visualized over the exposed myocardial surface, whereas sparse contact electrodes provide extracellular signals that are more directly related to those used in clinical electrophysiology[8,9,12]. Torso-tank recordings extend the measurements farther from the myocardium and provide an experimental representation of the electrical field available to BSPM and ECGi approaches[18–20]. Acquiring these signals during the same cardiac event allows differences between modalities to be evaluated without introducing variation from separate experiments or sequential recordings.

This complementarity was demonstrated most directly in the small-heart configuration. Optical and MEA-derived activation maps could be compared over corresponding myocardial regions during sinus rhythm and VT, while the surrounding torso-tank electrodes simultaneously recorded the remotely measured electrical field. The three measurements should not be expected to produce identical spatial patterns because they represent different electrophysiological quantities and spatial scales. This distinction was also observed in our previous work, in which agreement among optical, contact-electrical, torso-tank, and ECGi representations depended on the rhythm and mapping metric being evaluated[21]. The present platform retains these complementary measurements while extending the experimental framework beyond the original small-heart whole-organ preparation.

The large-heart whole-organ configuration extends synchronized optical and torso-tank recording to porcine and human hearts while preserving intact organ geometry. This differs from panoramic optical systems such as those described by Lee et al. and RHYTHM, which primarily address optical coverage and reconstruction[15,16], and from highly integrated systems such as POEMS, whose optical and electrical interfaces are incorporated into a geometry specifically designed for mouse hearts[17]. Torso-tank experiments in porcine hearts have previously combined epicardial electrodes, body-surface recordings, and optical mapping for ECGi validation[19,20]. In the present implementation, transparent electrode PCBs allow optical and torso-tank recordings to be obtained through the same tank interfaces while the preparation is maintained by independently controlled coronary perfusion. The representative pacing experiments demonstrate that synchronized multimodal acquisition can be maintained under different pacing conditions in intact human hearts, although the present data were not intended to provide a quantitative assessment of rate-dependent conduction.

The epi-endo configuration addresses a different limitation of whole-organ surface mapping. Activation within the ventricular wall may differ between the epicardial and endocardial surfaces, particularly during complex rhythms, and measurements obtained from one surface cannot necessarily be used to infer activity on the other[10,11]. By positioning the preparation between two optical fields and two contact-electrode arrays, the platform allows epicardial and endocardial activation to be recorded during the same cardiac event. The sinus-rhythm and fibrillation examples demonstrate that both organized and complex activation can be examined simultaneously from opposing myocardial surfaces. This configuration therefore complements whole-organ mapping by sacrificing intact global geometry in exchange for direct epi-endo access.

An additional objective of the platform was to reduce the practical complexity associated with operating several independent experimental systems. Optical acquisition, electrical acquisition, synchronization, pacing and arrhythmia-induction protocols, physiological monitoring, experimental metadata, and event logging were coordinated through a common graphical interface. A shared hardware timing signal linked the independent acquisition systems, while physiological measurements and experimental events were recorded within the same workflow. These features do not eliminate the technical requirements of ex vivo cardiac experimentation, but they reduce the number of independent operations required during an experiment and facilitate consistent association between the acquired datasets and experimental conditions. To support implementation by other laboratories, the control software, embedded firmware, electronic schematics, mechanical designs, and bill of materials are being made publicly available through the associated GitHub repository.

The three-dimensional reconstruction workflow provides an experiment-specific representation of external cardiac morphology that can support anatomical visualization and future registration of electrophysiological measurements. Unlike the panoramic reconstruction used in systems such as RHYTHM[16], electrophysiological maps were not yet systematically

registered onto the reconstructed surfaces in the present study. The method is also based on external silhouettes and therefore cannot recover internal structures or concavities that remain hidden throughout the rotational sequence. Its current role should consequently be considered morphological rather than a complete anatomical or electrophysiological reconstruction.

Overall, the platform brings together experimental approaches that are commonly implemented separately: panoramic optical mapping, contact-electrical mapping, torso-tank recording, epi-endo mapping, physiological monitoring, stimulation, and three-dimensional morphology reconstruction. Its principal contribution is therefore not a single new mapping modality, but an open-source experimental framework in which complementary measurements can be synchronized and adapted to different cardiac preparations. This provides a basis for studying complex arrhythmia mechanisms and for evaluating how features of myocardial activation are represented by electrical mapping techniques relevant to arrhythmia diagnosis and ablation.

Methods

Ethical approval and experimental models

Rabbit experiments were approved by the Ethics Committee on the Use of Animals of the Federal University of ABC, São Paulo, Brazil, under protocol 3947230519 and were performed in accordance with the relevant institutional guidelines and regulations. New Zealand White rabbits were obtained from an authorized commercial supplier. Before experimentation, the animals were housed under controlled environmental conditions with a 12-h light/dark cycle, an ambient temperature of approximately 22 °C, adequate ventilation, unrestricted access to water, and a balanced diet.

Porcine hearts were obtained from a certified surgical-training facility. The animals were approximately four months old and weighed 35–40 kg.

Human cardiac specimens were supplied by the Virginia Commonwealth University Heart Transplant Program. Donor hearts that had been declined for transplantation were surgically explanted by the cardiac-surgery team and used in this study under Institutional Review Board protocol HM11452.

The small-heart configuration was implemented using rabbit hearts, whereas the large-heart whole-organ and epi-endo configurations were implemented using porcine and human hearts.

Preparation, perfusion, and physiological monitoring

The perfusion system used across the three experimental configurations is shown in Fig. 5. The perfusate collected in a bulk reservoir was returned by a peristaltic pump to an elevated main reservoir and subsequently directed through one or two independently monitored perfusion lines. Each line contained an analog flow meter for visual inspection, a heat exchanger, an inline bubble trap, a digital flow and temperature sensor, and a pressure sensor positioned close to the preparation.

One perfusion line could terminate at either an aortic or coronary cannula, whereas the second line terminated at a coronary cannula. Small-heart whole-organ experiments used one line for retrograde aortic perfusion. Large-heart epi-endo experiments used one coronary line supplying the isolated ventricular preparation. Large-heart whole-organ experiments used both lines to perfuse the left and right coronary circulations independently.

Small-heart whole-organ preparation

Animals were sedated with buprenorphine (0.05 mg/kg, intramuscular). Approximately 30 min later, general anaesthesia was induced with ketamine (50 mg/kg, intramuscular) and xylazine (7 mg/kg, intramuscular). Anaesthetic depth was confirmed by absence of a withdrawal response to toe pinch, and supplementary anaesthetic was administered when required. Heparin (500 U/kg, intravenous) was administered through the marginal ear vein before thoracotomy. Following median sternotomy, the heart was rapidly excised while preserving sufficient ascending aorta for cannulation and was immediately transferred to cold, low-calcium solution. Pulmonary remnants, connective tissue, and excess surrounding tissue were removed. The aorta was then cannulated and the coronary circulation flushed to remove residual blood. Stable coronary perfusion was established within approximately 10 min of excision.

Small hearts were perfused retrogradely through the aorta using a modified constant-pressure Langendorff preparation[22,23]. The main reservoir was positioned approximately 100 cm above the level of the aortic cannula, corresponding to a nominal hydrostatic pressure of approximately 73 mmHg. Pressure measured close to the cannula was generally maintained between 60 and 70 mmHg. Coronary flow was typically 20–40 mL/min, depending on preparation size and coronary resistance.

Medical-grade silicone tubing with an outer diameter of approximately 6 mm and an inner diameter of approximately 4 mm was used in the perfusion circuit. Tubing between the heat exchanger and the preparation was kept short to minimize dead volume and heat loss. A 300-μL PEEK bubble trap fitted with a polytetrafluoroethylene membrane and 1/4–28 fluidic connections (PreciGenome, San Jose, CA, USA) was positioned upstream of the cannula.

The custom aortic cannula included circumferential grooves to improve mechanical retention of the ascending aorta and reduce leakage or displacement during prolonged recordings. A tin-plated copper conductive ring incorporated into the cannula remained in contact with the aortic region and was used as the reference electrode for the epicardial MEAs.

The modified Krebs–Henseleit solution contained, in mmol/L, 115 NaCl, 4.6 KCl, 25 $NaHCO_3$, 1.2 $CaCl_2{\cdot}2H_2O$, 1.2 KH_2PO_4, 1.2 $MgSO_4{\cdot}7H_2O$, 1 sodium pyruvate, and 11 glucose. The solution was continuously bubbled with carbogen (95% O_2/5% CO_2) and maintained at pH 7.40 $\pm$ 0.05, conductivity 13 $\pm$ 1 mS/cm, and temperature 37.5 $\pm$ 0.5 °C.

Custom cannula holders, tank interfaces, cable guides, sensor mounts, and optical-alignment components were manufactured by fused-filament 3D printing using PLA or PETG. Detailed mechanical drawings and fabrication parameters are provided in the Supplementary Information.

Large-heart whole-organ preparation

Pigs were initially anesthetized with Atropine 1.6 mg (0.04mg/kg) and Telazol 200 mg IM (3-5mg/kg). It was followed by maintaining them under a surgical plane of anesthesia with inhaled isoflurane throughout the experimental procedure. Intravenous fluids were administered continuously at a rate of 10 mL/kg/h. At the end of the procedure, euthanasia was performed by intravenous administration of Somnasol, a commercial euthanasia solution containing pentobarbital and phenytoin, according to the manufacturer's recommended dosage. A total of 390 mg of pentobarbital and 1 mL of the phenytoin-containing solution were administered intravenously.

Human hearts were surgically extracted by the cardiac surgery team during transplantation. Immediately upon removal, the hearts underwent perfusion with an ice-cold cardioplegic solution administered via both left and right coronary arteries to maintain myocardial integrity and minimize ischemic injury during transport to the laboratory for optical mapping studies. In preparation for these experiments, the intact heart model required independent perfusion of the left and right coronary arteries. Additionally, the marginal artery was cannulated and securely fixed with surgical silk ligature.Upon arrival in the laboratory, the left and right coronary ostia were identified and cannulated independently.

Each coronary cannula consisted of a blunt needle fitted with a conical silicone stopper. Different needle and stopper dimensions were used according to coronary diameter. The two cannulae were connected to separate perfusion lines supplied by the same main reservoir, allowing perfusion of the left and right coronary circulations to be adjusted independently according to their hydraulic resistance.

Large hearts were perfused at a nominal pressure of approximately 70 mmHg using oxygenated modified Tyrode solution maintained at approximately 37 °C and pH 7.4. The solution contained, in mmol/L, 128.20 NaCl, 4.70 KCl, 25 $NaHCO_3$, 1.2 $NaH_2PO_4{\cdot}H_2O$, 1.05 $MgCl_2{\cdot}6H_2O$, 10 glucose, and 1.8 $CaCl_2$. The solution was continuously bubbled with 95% O_2/5% CO_2 and was also used as the surrounding tank solution.

The heart was suspended inside the recording tank using an adjustable support. Height and orientation were adjusted to maintain optical access to the mapped epicardial regions and to prevent direct contact between the preparation and the torso-tank electrode interfaces. The large-heart whole-organ recording configuration is shown in Fig. 2A,B.

Large-heart epi-endo preparation

For the epi-endo studies of ventricular free wall from both pig and human hearts, it was necessary to separate the ventricle. Firstly, separate the pulmonary trunk from the aorta. Then, make an incision along the left anterior descending artery, starting through the pulmonary trunk. Then, extend the incision down to the apex of the heart, continuing along the posterior descending artery. After, identify the right coronary artery and make a transverse incision through the aorta, and completely transect the left ventricle. For the end, cannulate at the entry point of the right coronary artery. It allows to have the ventricular free-wall preparation isolated while preserving a coronary branch supplying the tissue. The vessel was cannulated and perfused with warmed, oxygenated modified Tyrode solution using one of the coronary perfusion lines.

The tissue was mounted approximately flat within a transparent acrylic chamber between two MEAs. One array contacted the epicardial surface and the other contacted the endocardial surface. The holder provided stable tissue–electrode contact without excessive compression and preserved optical access to both surfaces. The recording configuration and chamber are shown in Fig. 3A,B.

Physiological monitoring

Perfusion conditions were monitored continuously during the experiments. Coronary flow and inline perfusate temperature were measured using SLF3S-4000B digital liquid-flow sensors (Sensirion AG, Stäfa, Switzerland). Perfusion pressure was measured using HSCMRNV160MG2A3 digital gauge-pressure sensors (Honeywell International Inc., Charlotte, NC, USA) positioned close to the cannulation site and approximately at the same vertical level as the preparation to minimize hydrostatic offset.

Tank temperature was monitored independently using a K-type thermocouple connected to a MAX6675 thermocouple-to-digital converter. Large-heart experiments additionally incorporated fluid-level monitoring.

Each monitored perfusion line was associated with an Arduino Nano sensor node and an nRF24L01 wireless module. Measurements were transmitted to an ESP32-S3 gateway connected to the host computer. Sensor values were displayed numerically and as rolling time-series plots in the experimental-control software and stored with timestamps together with stimulation, synchronization, and recording events.

The firmware used in the present experiments was developed for the Arduino Nano and ESP32-S3 hardware. Other microcontrollers could be adapted provided that they support the required sensor and communication interfaces, although alternative implementations were not evaluated. Electronic wiring, communication protocols, and firmware implementation are described in the Supplementary Information.

Mapping

The platform combined optical, contact-electrical, and torso-tank measurements according to the preparation and experimental objective. Small-heart whole-organ experiments supported all three modalities, large-heart whole-organ experiments combined optical and torso-tank recordings, and the epi-endo preparation combined optical and contact-electrical mapping of opposing myocardial surfaces.

Optical mapping

Voltage-sensitive optical mapping was performed using Di-4-ANBDQPQ/JPW-6003. Camera number, lens selection, illumination geometry, and field of view were adapted to preparation dimensions and to the myocardial surfaces being investigated[8,9].

Small-heart panoramic optical mapping

Three synchronized HB-1800-S high-speed cameras (Emergent Vision Technologies, Austin, TX, USA) were positioned approximately 120° apart around the tank to provide panoramic epicardial coverage (Fig. 1A). Each camera was fitted with a CF25ZA-1S 25-mm C-mount lens (Fujinon, Saitama City, Japan).

Excitation was provided by six PT-39-DR-L51 deep-red LEDs (Luminus Devices, Sunnyvale, CA, USA) centred at approximately 650 nm. Each LED was coupled to an ACL2520U-A condenser lens and an FBH650-40 650/40-nm band-pass filter (Thorlabs, Newton, NJ, USA). Fluorescence was recorded through FF01-715/LP-22-D 715-nm long-pass filters (Semrock, Rochester, NY, USA).

The cameras incorporated Sony Pregius IMX425 global-shutter CMOS sensors with a nominal resolution of 1604×1100 pixels and 9-μm pixels. They were positioned approximately 9 cm above the base of the heart and 20–24 cm radially from the tank centre, depending on preparation size and position. All three cameras recorded ventricular tissue, while two views provided additional coverage of the left and right atria. Representative simultaneous camera images are shown in Fig. 1B.

Recordings were acquired simultaneously at 500 frames/s with an active resolution of 1600×1000 pixels and 12-bit depth. Typical recordings lasted 10 s and were acquired using StreamPix 9 software (NorPix, Montreal, QC, Canada).

A 1 mg/mL stock solution of Di-4-ANBDQPQ/JPW-6003 was prepared in ethanol[24]. For staining, 0.25 mg of dye was added to 150 mL of perfusate and recirculated through the coronary circulation for up to two cycles or until visually uniform epicardial staining was obtained.

Mechanical contraction was reduced using blebbistatin. An initial 75 mL volume of Krebs–Henseleit solution containing 20 μM blebbistatin was administered, followed by continuous perfusion at a maintenance concentration of 1.7 μM[9].

In selected experiments, saline-filled balloons were inserted into the atrial chambers to prevent collapse in the absence of physiological filling pressure. One balloon was introduced through the inferior vena cava into the right atrium and another through a pulmonary vein into the left atrium.

Large-heart whole-organ optical mapping

Large whole hearts were imaged using two DMK 37BUX287 high-speed cameras (The Imaging Source, Charlotte, NC, USA) positioned on opposite sides of the tank (Fig. 2A). The cameras imaged opposing epicardial regions through the transparent tank walls and transparent electrode PCBs.

Depending on preparation dimensions and camera distance, either a 12-mm $f/1.2$ or 6-mm $f/1.4$ lens was used. Illumination was provided by high-power red LEDs centred at approximately 650 nm. Six LEDs were used in most whole-heart experiments, although their positions were adjusted according to preparation orientation and optical access. Excitation light was filtered using 650/40-nm band-pass filters, and emitted fluorescence was collected through long-pass emission filters.

Optical recordings were acquired at 500 frames/s with a resolution of 720×540 pixels using StreamPix 10. Both optical streams were synchronized with the corresponding electrical recordings and stimulation markers.

Large hearts were stained with 1 mg of Di-4-ANBDQPQ/JPW-6003. An initial 200 mL volume of modified Tyrode solution containing 25 μM blebbistatin was delivered to reduce contraction, followed by a maintenance concentration of 3 μM in the circulating solution.

Large-heart epi-endo optical mapping

The epi-endo configuration used two optical pathways to map opposing ventricular surfaces (Fig. 3A). One camera imaged the endocardial surface directly from above. Epicardial fluorescence was reflected by a mirror positioned at approximately 45° toward the second camera.

Four red excitation LEDs were positioned around the preparation to illuminate both surfaces while limiting obstruction by the MEAs. Camera, mirror, illumination, and electrode positions were adjusted so that the optical fields overlapped the regions covered by the epicardial and endocardial arrays. Both optical streams were linked to the same synchronization system used for the whole-heart configurations.

Contact electrical mapping

Small hearts

Three custom flexible MEAs were used for epicardial electrical mapping. Each array contained 16 platinum electrodes, providing 48 recording sites in total. One array was positioned on the left atrium, one on the right atrium, and one on the ventricular epicardium.

The two atrial arrays were fabricated on flexible polyethylene terephthalate substrates measuring approximately 14×9.5 mm with an inter-electrode spacing of approximately 2 mm. The ventricular array measured approximately 19×22 mm and used approximately 3-mm vertical and 6-mm horizontal spacing. Array dimensions are shown in Fig. 1A.

The flexible substrates partially conformed to the curved epicardial surface. Arrays were positioned under direct visual guidance, and contact pressure was limited to that required for stable electrical coupling.

Two Intan RHD 64-channel headstages were used for acquisition. One received two 16-channel MEAs and the second received the remaining array. Signals were sampled at 4 kHz using Open Ephys. The conductive ring incorporated into the aortic cannula served as the reference electrode.

Large-heart epi-endo preparation

The epi-endo configuration used two custom 16-electrode platinum–iridium MEAs arranged as 4×4 grids with approximately 10-mm inter-electrode spacing in both directions. The arrays were constructed using electrode components repurposed from medical cardiac catheters.

One array contacted the epicardial surface and the second contacted the endocardial surface. The 32 signals were acquired using an Intan RHD headstage, with a reference electrode positioned in the surrounding solution.

Four custom needle electrodes, designated L1–L4, were positioned at spatially separated locations to obtain broader ECG-like signals from the preparation. These signals were recorded using a PowerLab 16/30 system. Electrode placement is shown schematically in Fig. 3A.

Torso-tank electrical mapping

Small hearts

Torso-tank potentials from small hearts were recorded using a custom hexagonal acrylic tank developed as a torso analogue[21]. The geometry and principal dimensions of the tank are shown in Fig. 1A.

Ten recording electrodes were distributed over each of the six planar tank faces, providing 60 torso-tank channels. The central region of each face was left free of electrodes to maintain optical access to the preparation.

The heart was suspended near the geometric centre of the tank. The surrounding solution contained, in mmol/L, 23 NaCl and 260 sucrose. Its electrical resistivity was adjusted to approximately 500 $\Omega \cdot$cm under the experimental measurement conditions. The tank solution was circulated at approximately 100 mL/min and maintained at 37–38 °C.

Initial versions of the tank used 10-mm stainless-steel electrodes. The final configuration used sintered Ag/AgCl electrodes, which provided improved baseline stability during prolonged recordings.

The 60 tank electrodes were connected to an Intan RHD 64-channel headstage (Intan Technologies, Los Angeles, CA, USA) through custom wiring and 36-pin adapters. Signals were sampled at 4 kHz using Open Ephys. Unused headstage inputs were connected to the appropriate reference or ground lines rather than being left electrically floating.

Torso-tank potentials were acquired in a unipolar configuration using a custom Wilson-central-terminal and common-mode feedback circuit. Tank connections corresponding approximately to the conventional left-arm, right-arm, and left-leg positions contributed to the Wilson central terminal, whereas the right-leg-equivalent connection was used for common-mode feedback.

Large hearts

Large-heart torso-tank recordings were obtained using two removable transparent electrode PCBs positioned on opposite sides of the recording tank (Fig. 2A).

Each PCB contained fifteen circular silver-plated electrodes approximately 10 mm in diameter, arranged in five rows of three. The two interfaces therefore provided 30 torso-tank recording positions. PCB dimensions and electrode distribution are shown in Fig. 2A.

The transparent substrates allowed the electrode interfaces to remain between the cameras and the preparation while preserving optical access to the heart. Signals from the two boards were acquired using an Intan RHD 64-channel headstage and an Intan RHD Recording Controller. The electrical reference was positioned in contact with the aortic region.

Torso-tank potentials, optical fluorescence, stimulation markers, and synchronization signals were acquired during the same recording intervals.

Experimental Management Software, synchronization, and data acquisition

A custom experimental-control interface implemented in Python using Tkinter was used to coordinate recording, synchronization, stimulation, physiological monitoring, metadata entry, annotations, and data logging (Fig. 6). Configuration-specific versions of the software shared the same core functions.

The purpose of the synchronization system was to ensure that optical and electrical measurements acquired by independent devices could be related to the same cardiac event. A 500-Hz TTL pulse train generated by the timing controller was used as the common hardware reference. Each rising edge triggered acquisition of one optical frame. Camera exposure was configured independently and was not determined by the duty cycle of the synchronization waveform.

The same synchronization signal was recorded by the electrical acquisition system. Optical frame indices could therefore be associated with electrical sample indices using the recorded trigger edges rather than relying on independent software timestamps.

The GUI communicated with an ESP32-S3 gateway through USB serial communication. Synchronization and stimulation commands were transmitted through the gateway to the associated control hardware, while physiological measurements and hardware-status information were returned to the computer for display and storage. Timing-critical synchronization signals were generated by a Teensy 4.1 controller.

The software displayed physiological measurements, synchronization state, stimulation parameters, and acquisition status during the experiment. Experimental metadata included specimen information, acquisition settings, stimulation parameters, pharmacological interventions, and contextual notes.

Recording start and stop events, stimulation commands, synchronization changes, physiological measurements, and operator annotations were written to timestamped log files. Optical and electrical acquisition directories were also monitored so that generated data files could be associated with the corresponding experimental record.

The communication between the control software, embedded controllers, physiological-monitoring nodes, and acquisition systems is summarized in Supplementary Fig. S3. Implementation-level details of the serial communication, firmware, background processes, hotkeys, directory monitoring, and synchronization commands are provided in the GitHub Repository.

Arrhythmia induction and pacing protocols

Small hearts were stimulated using a custom single-channel constant-current stimulator based on a discrete PNP-transistor current mirror, open-source available. The circuit provided an experimentally used output range of approximately 1–45 mA and an effective compliance voltage of approximately 35 V. Four series-connected 9-V batteries provided an isolated supply. Stimulation was delivered through a custom bipolar pacing catheter with approximately 2-mm inter-electrode spacing.

Triggering was optically isolated from the stimulation output. Component-level circuit design, transistor selection, current-setting circuitry, and the complete schematic are provided in the Supplementary Information.

Before each stimulation protocol, capture threshold was determined by gradually increasing stimulation current until consistent myocardial activation was observed in the electrical recordings and, when available, the optical signals. Regular pacing was subsequently used to establish controlled activation sequences and confirm capture.

For S1–S2 protocols, ten S1 stimuli were delivered using a pulse width of 2 ms and a cycle length of 250 ms. The S1 train was followed by one premature S2 stimulus. The initial S1–S2 interval was approximately 220 ms and was shortened in 10-ms steps until capture was lost or an arrhythmia was induced.

For selected arrhythmia-induction experiments, 1 μM carbachol was added to the perfusate. Rapid stimulation consisted of three trains of 100 pulses delivered at 50 Hz, with approximately 2 s between consecutive trains.

Large hearts were stimulated using an A365 Constant Current Stimulus Isolator (World Precision Instruments, Sarasota, FL, USA), providing bipolar constant-current stimulation up to 10 mA with a compliance voltage of 100 V. Baseline pacing, programmed stimulation, and burst pacing were used according to the experimental protocol. In the representative whole-heart experiment shown in Fig. 2C, the same preparation and pacing site were recorded at cycle lengths of 350 and 500 ms.

Three-dimensional heart morphology reconstruction

External cardiac morphology was reconstructed after selected whole-heart experiments using rotational imaging. The reconstruction workflow is shown in Fig. 4.

For large-heart reconstruction, camera calibration was performed using the MC-Calib framework and a calibration object containing ChArUco patterns[25]. The calibration object was positioned at the location subsequently occupied by the preparation.

Following electrophysiological acquisition, the heart was rotated through approximately 100 angular positions over 360°. Rotation was produced using a stepper-motor system while images were acquired from a fixed camera geometry. Images were acquired with high contrast between the cardiac silhouette and the background.

The cardiac outline was segmented semi-automatically at each rotational position. Silhouettes were corrected for camera tilt and rotational misalignment before being combined in the calibrated three-dimensional coordinate system. Their intersection constrained the external volume occupied by the preparation.

The resulting volume was converted into a triangulated surface mesh and refined to remove isolated regions, segmentation irregularities, and support-related artefacts[26]. The sequence from calibration and rotational imaging to silhouette correction and final surface generation is illustrated in Fig. 4.

The reconstructed mesh represents the external cardiac morphology. Internal anatomy and concavities that remained hidden throughout the rotational sequence could not be recovered.

For small-heart experiments, rotational reconstruction was performed using the previously developed single-camera workflow[16,21]. Details of the small-heart calibration object, rotational hardware, and acquisition system are provided in the Supplementary Information.

Signal preprocessing and electrophysiological analysis

All signal processing was performed in MATLAB. Optical and electrical recordings were processed according to their acquisition characteristics and aligned using the recorded synchronization signal.

Small-heart optical recordings were spatially binned using an 8×8-pixel factor. A 4×4-pixel binning factor was used for large-heart recordings. A Gaussian filter with a 5×5 spatial kernel and a 1×7 temporal kernel was subsequently applied. Low-frequency baseline drift was removed using a zero-phase high-pass Butterworth filter with a cutoff frequency of 0.5 Hz.

Fluorescence was expressed relative to baseline as

$$\frac{\Delta F}{F_0} = \frac{F - F_0}{F_0} \times 100\% \tag{1}$$

where F is the instantaneous fluorescence intensity and F_0 is the baseline fluorescence. Optical recordings acquired at 500 Hz were resampled to 4 kHz using linear interpolation when direct temporal comparison with the electrical recordings was required.

MEA and torso-tank signals were high-pass filtered at 0.5 Hz using zero-phase Butterworth filtering. Power-line interference was attenuated using a fourth-order infinite-impulse-response notch filter centred at 60 Hz, followed by low-pass filtering at 250 Hz. Channels were inspected for disconnection, saturation, baseline instability, and persistent common-mode contamination before mapping.

Local activation time (LAT) was defined according to recording modality because optical fluorescence and extracellular electrograms represent different electrophysiological quantities[8,21]. Optical LAT was assigned to the time at which the fluorescence upstroke reached 50% of its amplitude. For MEA electrograms, LAT was assigned to the maximum negative temporal derivative:

$$\mathrm{LAT}_{\mathrm{MEA}} = \arg\max_{t} \left(-\frac{dV(t)}{dt} \right) \tag{2}$$

MEA-derived LAT values were spatially interpolated using Laplacian interpolation when continuous maps were required. For the small-heart comparisons shown in Fig. 1C,D, the electrode measurements were interpolated onto a 5×5 grid corresponding to the optical region covered by the MEA.

Torso-tank recordings were analyzed separately because they represent remotely measured electrical activity rather than local myocardial activation. Waveform timing was characterized using the temporal centre of mass of the cumulative absolute potential:

$$t_{\mathrm{COM}} = \min \left\{ t : \int_{t_0}^{t} |V(\tau)|\, d\tau \geq \frac{1}{2} \int_{t_0}^{t_1} |V(\tau)|\, d\tau \right\}, \tag{3}$$

where t_0 and t_1 delimit the analyzed cardiac event. The resulting t_{COM} value was treated as a temporal descriptor of the torso-tank waveform rather than as a local activation time at the tank wall.

For small-heart recordings, the timing values were interpolated over an unfolded representation of the tank surface to generate the distribution shown in Fig. 1E. For large-heart whole-organ recordings, the two transparent PCB interfaces were processed independently to generate timing distributions for the opposing tank faces.

The optical and torso-tank maps obtained at pacing cycle lengths of 350 and 500 ms in Fig. 2C were independently referenced in time. They were therefore used to compare the spatial activation and timing distributions within each pacing condition rather than absolute activation times between the two recordings.

Conclusions

We developed the first open-source platform for synchronized multimodal investigation of ex vivo perfused hearts and demonstrated its use in small-heart whole-organ, large-heart whole-organ, and large-heart epi-endo preparations. The platform combines optical, contact-electrical, and torso-tank mapping with controlled perfusion, physiological monitoring, pacing and arrhythmia induction, experimental synchronization, and centralized data recording. Its implementation in rabbit, porcine, and human hearts demonstrates that the same experimental framework can support complementary mapping strategies across different preparation sizes and recording geometries. By enabling optical and electrical measurements to be acquired during the same cardiac events, the platform provides an experimental basis for investigating complex arrhythmia mechanisms and for evaluating cardiac mapping approaches relevant to electrophysiological diagnosis and ablation. Public availability of the software, firmware, electronic designs, and mechanical files is intended to facilitate reproduction and adaptation of the platform by other research groups.

Data availability

The datasets generated and analyzed during the current study are available from the corresponding author upon reasonable request. Analysis scripts are maintained in a private institutional repository and can be made available subject to institutional and ethical restrictions. The full schematics for the supports, stimulators, tank, and MEAs and also The code for the control boards, sensors, and main control GUI are in the following GitHub repository: https://github.com/HEartLab-ufabc/HEartLab-Multimodal-Mapping.git.

Acknowledgements

This work was supported by the São Paulo Research Foundation (FAPESP), grant 2018/25606-2, and CNPq INCT INTERAS 406761/2022-1. J.Si. was supported by FAPESP grant 2020/03601-9, A.Q. was supported by FAPESP grant 2023/06306-6. T.N. was supported by FAPESP grant 2024/02521-2. M.L was supported by FAPESP grant 2025/22698-7. S.E. and J.G were supported by CAPES. The large-heart studies were additionally supported by the Dr. Kenneth Ellenbogen Endowment. The authors also thank the Virginia Commonwealth University cardiac-surgery team for their support in providing explanted human hearts used in the large-heart experiments.

Author contributions statement

V.S. developed the experimental-control software, contributed to hardware design and integration, implemented the experimental platform, performed data analysis and visualization, and drafted the manuscript. T.N. contributed to the development of the updated tank and Wilson central terminal, participated in experimental data acquisition, and prepared figures for the manuscript. J.Si. developed the multi-electrode arrays, contributed to experimental data acquisition, signal processing, data analysis and visualization, and reviewed and edited the manuscript. M.L. implemented the physiological sensor network for the small-heart configuration. J.G. and S.E. contributed to experimental data acquisition. I.U. supervised the large-heart experiments, contributed to adaptation of the platform, experimental design and interpretation, and reviewed and edited the manuscript. J.Sa. obtained the grant and scholarships for the platform development,conceived the study, supervised the development of the project, performed and supervised the experiments with rabbit, contributed to experimental design and interpretation of the results, and edited and reviewed the manuscript. All authors reviewed and approved the final manuscript.

Additional information

Competing interests: The authors declare no competing interests.

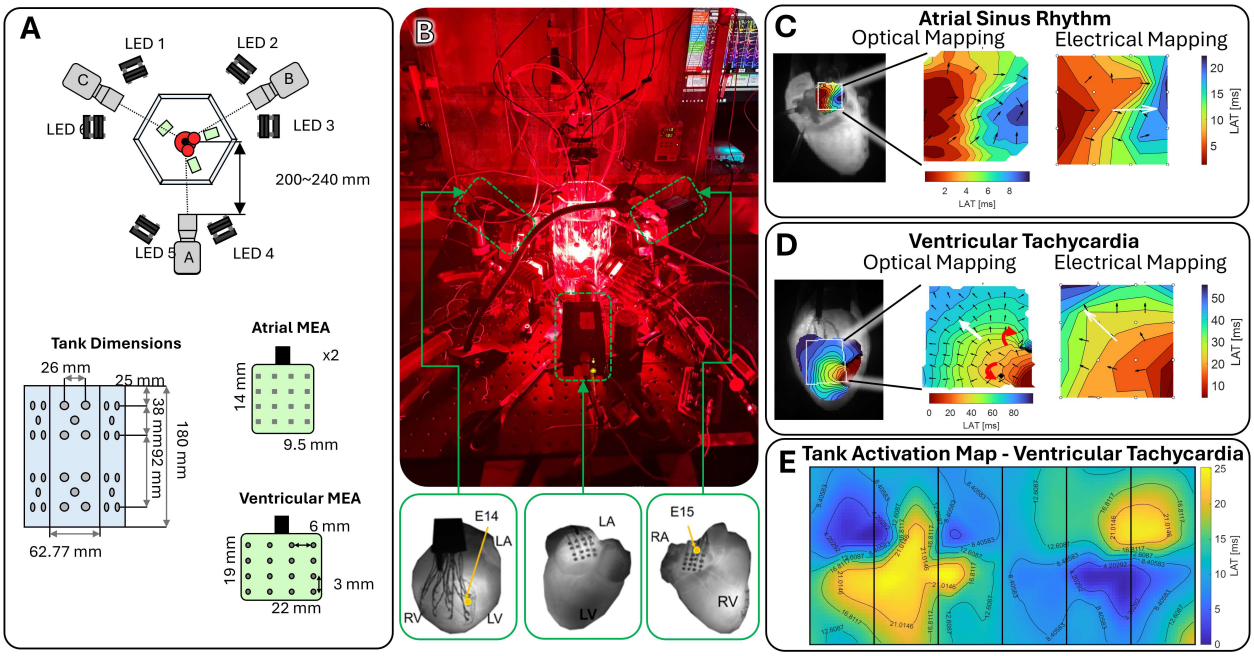


Figure 1. Small-heart configuration and representative multimodal activation maps. **(A)** Small-heart optical and electrical mapping geometry. Three cameras were positioned approximately 120° apart around the hexagonal tank, and six excitation LEDs illuminated the preparation. Tank and atrial and ventricular MEA dimensions are shown below. **(B)** Platform during an experiment and representative images acquired simultaneously by the three cameras. **(C)** Right-atrial local-activation-time (LAT) maps during sinus rhythm. From left to right: optical LAT map over the MEA-covered region, enlarged optical LAT map, and MEA-derived LAT map interpolated onto a 5×5 grid using Laplacian interpolation. **(D)** Optical and MEA-derived LAT maps during ventricular tachycardia, displayed in the same order. Dark orange indicates earlier activation and blue later activation. **(E)** Tank timing map obtained from the tank electrodes during the same ventricular-tachycardia episode, with blue indicating earlier and yellow later timing.

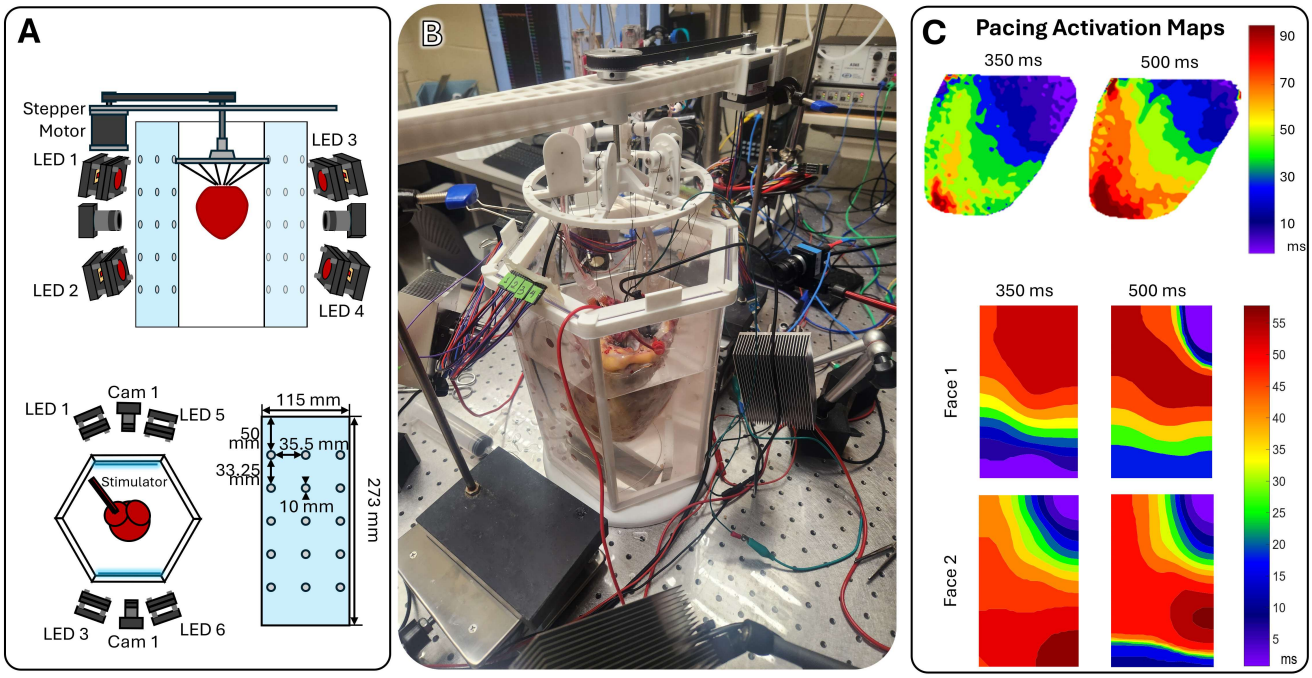


Figure 2. Large-heart whole-organ configuration and representative multimodal activation maps. **(A)** Large-heart whole-organ mapping geometry with two opposing cameras, circumferential excitation LEDs, and transparent PCBs containing silver-plated tank electrodes. For schematic proposal just two tank-fazes are sown. Four LEDs are shown for clarity, although six were used in most experiments. The dimensions and electrode distribution of the transparent PCB are also shown. **(B)** Platform during an experiment with an ex vivo perfused human heart. The preparation was positioned within the transparent tank between the opposing optical views and tank-electrode interfaces. **(C)** Representative activation maps from a human heart during pacing with cycle lengths of 350 and 500 ms. Optical maps are shown in the upper row, and tank electrical maps obtained from the two opposing PCB interfaces are shown below.

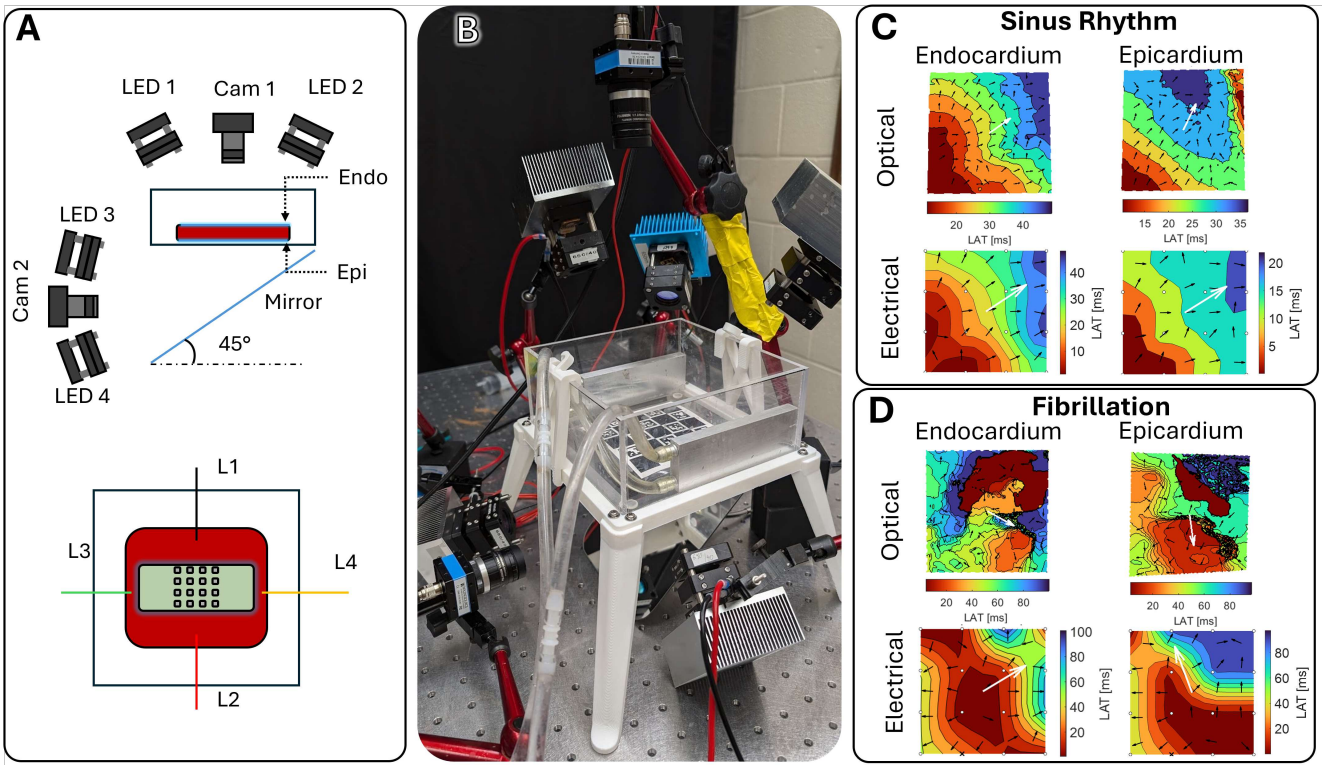


Figure 3. Large-heart epi-endo configuration and representative dual-surface activation maps. **(A)** Epi-endo mapping geometry with the ventricular preparation positioned between epicardial and endocardial MEAs. The endocardium was imaged directly, whereas epicardial fluorescence was reflected by a mirror positioned at approximately 45° toward the second camera. Needle electrodes L1–L4 provided additional electrical recordings. **(B)** Experimental platform before placement of the cardiac preparation, showing the transparent chamber, paired MEAs, illumination components, direct optical pathway, and mirror-assisted optical pathway. **(C)** Local-activation-time maps during sinus rhythm. Endocardial maps are shown in the left column and epicardial maps in the right column; optical maps are shown above the corresponding contact-electrical maps. **(D)** Optical and contact-electrical activation maps during fibrillation, presented for the same opposing surfaces. Red indicates earlier activation and blue later activation within the displayed temporal scale.

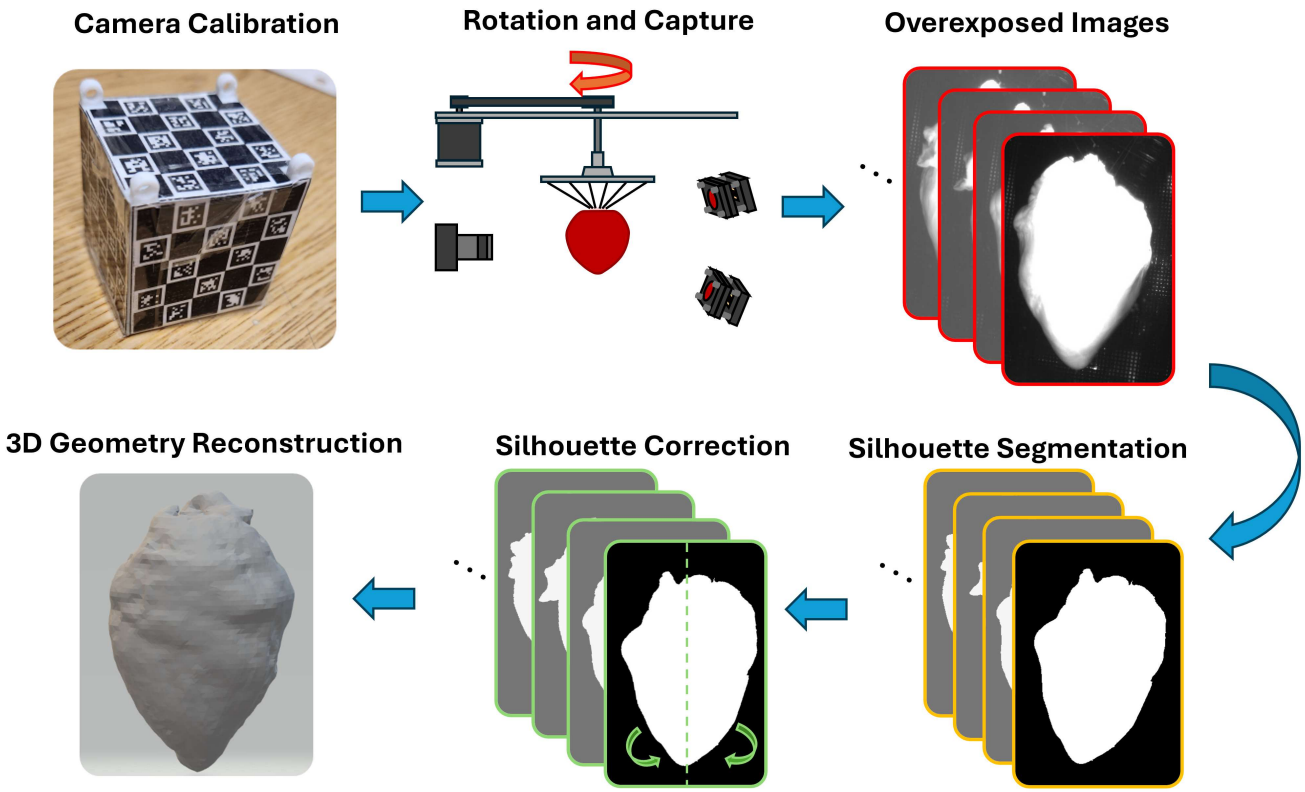


Figure 4. Rotational imaging and three-dimensional reconstruction workflow. Camera calibration was performed using a ChArUco calibration object positioned within the reconstruction volume. Following electrophysiological acquisition, the preparation was rotated through a sequence of angular positions using a stepper-motor system while images were acquired from a fixed camera geometry. Cardiac silhouettes were segmented from the rotational images, corrected for geometric and rotational misalignment, and combined to estimate the volume occupied by the preparation. The reconstructed volume was subsequently converted into a triangulated three-dimensional surface mesh and refined to reduce segmentation and support-related artefacts.

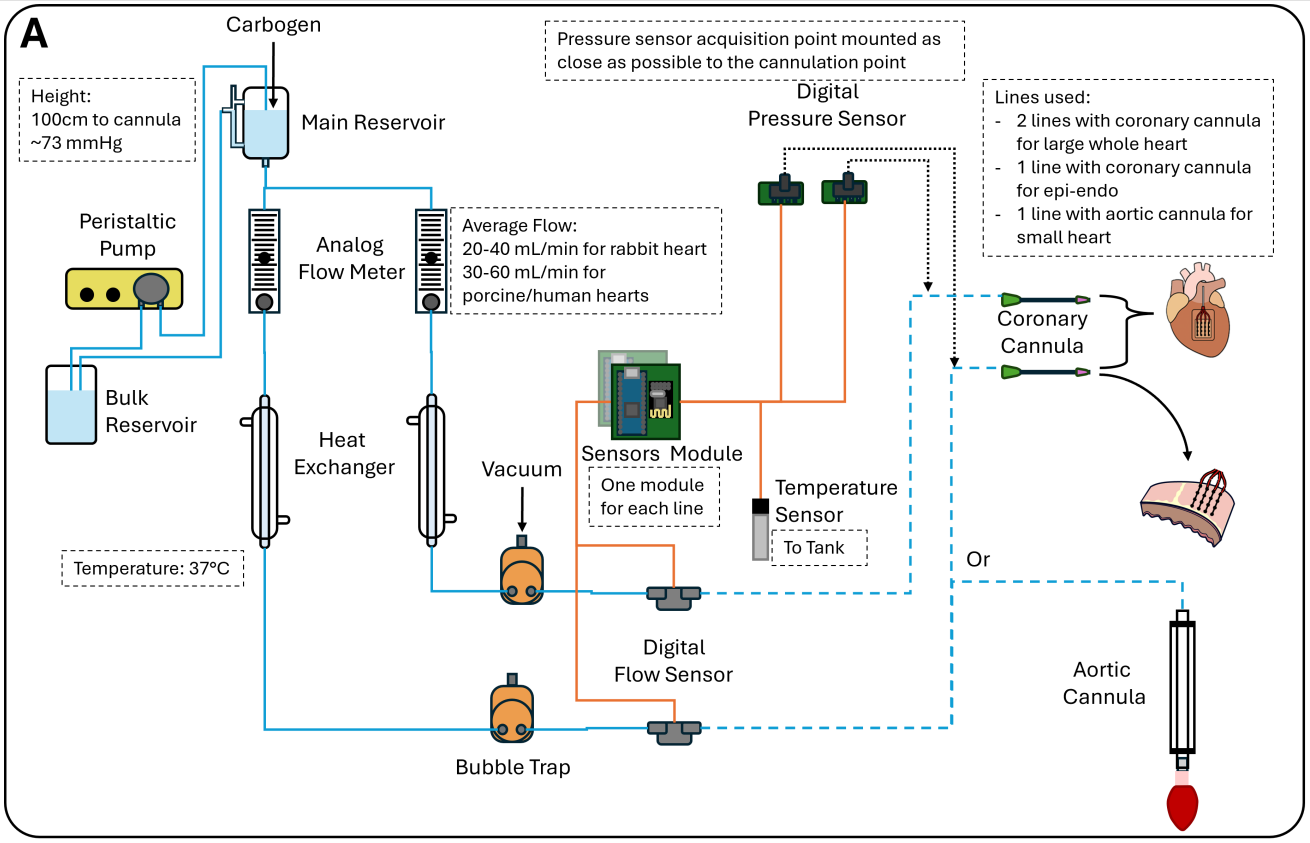


Figure 5. Shared perfusion architecture for small- and large-heart preparations. The perfusion system used a common bulk reservoir, peristaltic pump, and elevated main reservoir supplying two independently monitored perfusion lines. Each line incorporated an analog flow meter, heat exchanger, bubble trap, digital flow and temperature sensor, and pressure sensor. One line could be directed either to an aortic cannula or to a coronary cannula, whereas the second line supplied a coronary cannula. Small-heart whole-organ experiments used one aortic line, large-heart epi-endo experiments used one coronary line, and large-heart whole-organ experiments used two independently cannulated coronary lines. Each perfusion line was monitored by a dedicated Arduino Nano sensor node with nRF24L01 wireless communication. Representative temperature, flow, and perfusion-pressure parameters are indicated in the schematic.

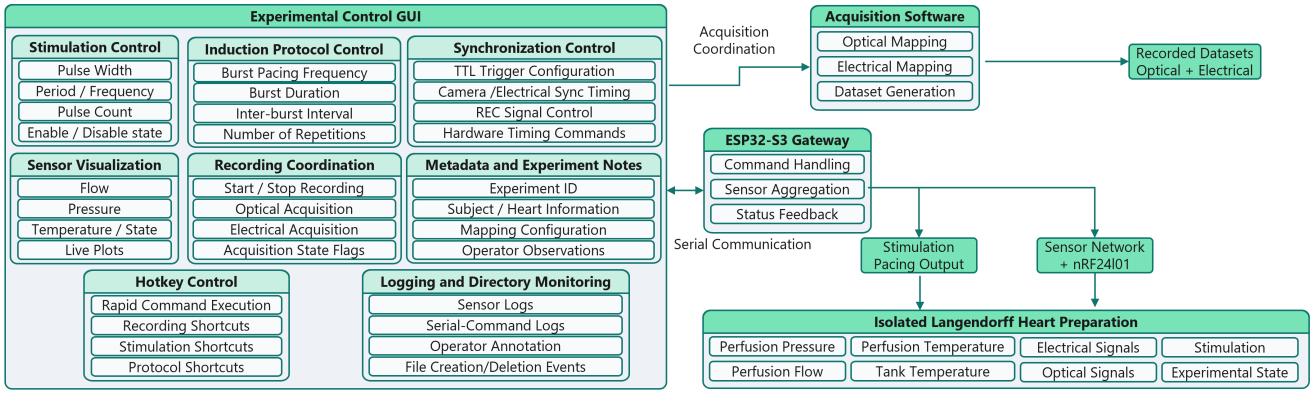


Figure 6. Experimental-control graphical user interface. The Python/Tkinter interface centralized recording control, synchronization, stimulation and induction protocols, physiological-sensor visualization, metadata entry, hotkey operation, event logging, and acquisition-directory monitoring. Communication with the ESP32-S3 gateway was performed through USB serial connection, allowing synchronization commands, sensor measurements, and hardware-status information to be exchanged. The interface also coordinated the optical and electrical acquisition software running on the host computer. Continuous serial reception, sensor updating, and directory monitoring were handled independently from the main graphical interface to maintain responsiveness during experiments.

References

1. Antzelevitch, C. & Burashnikov, A. Overview of basic mechanisms of cardiac arrhythmia. *Cardiac Electrophysiol. Clin.* **3**, 23–45 (2011).

2. Borlich, M. & Sommer, P. Cardiac mapping systems: Rhythmia, topera, ensite precision, and carto. *Cardiac Electrophysiol. Clin.* **11**, 449–458, DOI: 10.1016/j.ccep.2019.05.006 (2019).

3. Narayan, S. M. & John, R. M. Advanced electroanatomic mapping: Current and emerging approaches. *Curr. Treat. Options Cardiovasc. Medicine* **26**, 69–91, DOI: 10.1007/s11936-024-01034-6 (2024).

4. Stevenson, W. G. & Soejima, K. Recording techniques for clinical electrophysiology. *J. Cardiovasc. Electrophysiol.* **16**, 1017–1022 (2005).

5. Spach, M. S., Miller, W. T., Miller-Jones, E., Warren, R. B. & Barr, R. C. Extracellular potentials related to intracellular action potentials during impulse conduction in anisotropic canine cardiac muscle. *Circ. Res.* **45**, 188–204 (1979).

6. Joglar, J. A., Chung, M. K., Armbruster, A. L. *et al.* 2023 acc/aha/accp/hrs guideline for the diagnosis and management of atrial fibrillation: A report of the american college of cardiology/american heart association joint committee on clinical practice guidelines. *Circulation* **149**, e1–e156, DOI: 10.1161/CIR.0000000000001193 (2024).

7. Natale, A. *et al.* Catheter ablation for atrial fibrillation: indications and future perspective. *Eur. Hear. J.* **45**, 4383–4398, DOI: 10.1093/eurheartj/ehae618 (2024).

8. Efimov, I. R., Nikolski, V. P. & Salama, G. Optical imaging of the heart. *Circ. Res.* **95**, 21–33 (2004).

9. O'Shea, C. *et al.* Cardiac optical mapping: State-of-the-art and future challenges. *The Int. J. Biochem. & Cell Biol.* **126**, 105804 (2020).

10. Harada, T. *et al.* Simultaneous optical mapping system of endocardial and epicardial excitation. In *2014 36th Annual International Conference of the IEEE Engineering in Medicine and Biology Society*, 2853–2856, DOI: 10.1109/EMBC.2014.6944218 (2014).

11. Hansen, B. J. *et al.* Atrial fibrillation driven by micro-anatomic intramural re-entry revealed by simultaneous sub-epicardial and sub-endocardial optical mapping in explanted human hearts. *Eur. Hear. J.* **36**, 2390–2401, DOI: 10.1093/eurheartj/ehv233 (2015).

12. Knisley, S. B. & Neuman, M. R. Simultaneous electrical and optical mapping in rabbit hearts. *Annals Biomed. Eng.* **31**, 32–41 (2003).

13. Chowdhury, R. A. *et al.* Concurrent micro- to macro-cardiac electrophysiology in myocyte cultures and human heart slices. *Sci. Reports* **8**, 6947, DOI: 10.1038/s41598-018-25170-9 (2018).

14. Xu, L. *et al.* 3d multifunctional integumentary membranes for spatiotemporal cardiac measurements and stimulation across the entire epicardium. *Nat. Commun.* **5**, 3329, DOI: 10.1038/ncomms4329 (2014).

15. Lee, P. *et al.* Low-cost optical mapping systems for panoramic imaging of complex arrhythmias and drug-action in translational heart models. *Sci. Reports* **7**, 43217, DOI: 10.1038/srep43217 (2017).

16. Gloschat, C. *et al.* RHYTHM: An open source imaging toolkit for cardiac panoramic optical mapping. *Sci. Reports* **8**, 2921 (2018).

17. Rieger, M. *et al.* Enabling comprehensive optogenetic studies of mouse hearts by simultaneous opto-electrical panoramic mapping and stimulation. *Nat. Commun.* **12**, 5804, DOI: 10.1038/s41467-021-26039-8 (2021).

18. Ramanathan, C., Ghanem, R. N., Jia, P., Ryu, K. & Rudy, Y. Noninvasive electrocardiographic imaging for cardiac electrophysiology and arrhythmia. *Nat. Medicine* **10**, 422–428 (2004).

19. Bear, L. R. *et al.* Optical imaging of ventricular action potentials in a torso tank: A new platform for non-invasive electrocardiographic imaging validation. *Front. Physiol.* **10**, 146, DOI: 10.3389/fphys.2019.00146 (2019).

20. Bear, L. R. *et al.* Cardiac electrical dyssynchrony is accurately detected by noninvasive electrocardiographic imaging. *Hear. Rhythm.* **15**, 1058–1069, DOI: 10.1016/j.hrthm.2018.02.024 (2018).

21. Siles, J. *et al.* An integrated platform for 2-d and 3-d optical and electrical mapping of arrhythmias in langendorff-perfused rabbit hearts. *The J. Physiol.* (2025).

22. Langendorff, O. Untersuchungen am überlebenden säugethierherzen. *Pflügers Arch. für die gesamte Physiol. des Menschen und der Tiere* **61**, 291–332 (1895).

23. Skrzypiec-Spring, M., Grotthus, B., Szelag, A. & Schulz, R. Isolated heart perfusion according to langendorff—still viable in the new millennium. *J. Pharmacol. Toxicol. Methods* **55**, 113–126 (2007).

24. Lee, P. *et al.* In situ optical mapping of voltage and calcium in the heart. *PLoS ONE* **7**, e42562 (2012).

25. Rameau, F., Park, J., Bailo, O. & Kweon, I. S. MC-Calib: A generic and robust calibration toolbox for multi-camera systems. *Comput. Vis. Image Underst.* **217**, 103353, DOI: 10.1016/j.cviu.2021.103353 (2022).

26. Kazhdan, M., Bolitho, M. & Hoppe, H. Poisson surface reconstruction. In *Proceedings of the Fourth Eurographics Symposium on Geometry Processing*, 61–70 (2006).

Supplementary Methods

Physiological sensor modules and wireless communication

Each active perfusion line was associated with a dedicated sensor module based on an Arduino Nano and an nRF24L01 2.4-GHz transceiver. Distributed acquisition was used to reduce cabling around the preparation and allow individual perfusion lines to be monitored independently.

Coronary flow and inline perfusate temperature were measured using an SLF3S-4000B digital liquid-flow sensor (Sensirion AG). The sensor communicates through I^2C and provides both flow rate and fluid temperature from the same inline device. Perfusion pressure was measured using a Honeywell digital pressure sensor connected through I^2C and converted to mmHg by the Arduino firmware. Tank temperature was measured independently using a K-type thermocouple and MAX6675 thermocouple interface.

The Arduino firmware periodically acquired the sensor values and converted them to integer values with a scale factor of 100 before transmission. This reduced packet size while retaining two decimal places of resolution. The supplied sensor firmware transmitted a new packet every 200 ms.

Sensor packets were transmitted to the central controller through the nRF24L01 modules. The radio interface used SPI locally between the Arduino Nano and nRF24L01, with acknowledgement and retransmission enabled to improve reliability. Each node was assigned an identifier so that measurements from different perfusion lines could be distinguished by the receiver.

An ESP32-S3 acted as the communication gateway between the wireless sensor network and the host computer. Received packets were identified, formatted as text messages, and forwarded through USB serial communication. The GUI converted the transmitted integer values back to physical units, displayed them numerically and graphically, and optionally stored them in CSV files together with timestamps and optical/electrical recording-state flags.

Embedded control and synchronization

Embedded control was divided between the ESP32-S3 communication gateway and a Teensy 4.1 timing controller. The host computer communicated with the ESP32-S3 through USB serial at 2,000,000 baud. A text-based command protocol was used for stimulation, synchronization, sensor communication, and status messages because it allowed commands to be inspected directly during experimental setup and troubleshooting.

The ESP32-S3 firmware parsed commands received from the GUI and routed timing-critical commands to the Teensy through a hardware UART connection at 115,200 baud. It also received sensor packets from the wireless network and returned sensor and hardware-status messages to the computer.

The Teensy firmware generated three independently configurable TTL synchronization outputs and a separate recording-control signal. Synchronization channels could be configured in frequency, phase, and duty cycle using commands of the form `SET_SYNC <channel> <frequency> <phase> <duty>`. Individual outputs could then be enabled or disabled using `SYNC_START` and `SYNC_STOP` commands.

For optical acquisition, the principal synchronization signal was configured at 500 Hz. Its rising edges triggered the optical cameras and were recorded by the electrical acquisition system, providing a hardware reference between optical frame number and electrical sample number.

The recording-control command `SYNC_REC N` generated a recording interval referenced to a defined number of SYNC1 pulses. This allowed acquisition duration to be expressed directly in optical frames rather than relying only on software timing.

The Teensy firmware also included a digital stimulation output. Continuous pacing and burst sequences were generated using hardware timers rather than software delay loops. Stimulation parameters were transmitted as pulse width, period, pulse count, and enable state. The digital output provided the timing signal for the isolated analogue stimulation circuit described below.

Experimental-control software

The experimental-control software was implemented in Python using Tkinter. The program was separated into independent modules rather than implemented as a single script.

`main.py` initializes the Tkinter environment, serial interface, and main control window. `serial_handler.py` provides serial-port discovery, connection management, and communication with the ESP32-S3. `stimulation_gui.py` contains the principal experimental-control interface and coordinates stimulation, recording, synchronization, sensors, logging, and external acquisition software.

The stimulation interface provides one continuous pacing configuration (S0) and four programmable burst stages (S1–S4). Pulse width, period, number of pulses, and enable state are converted into structured serial commands and transmitted to the embedded controller. A separate `induction_protocol_window.py` module allows frequency, period, pulse width, duration, number of repeated bursts, and inter-burst interval to be configured. Frequency and period are linked automatically to prevent inconsistent parameter entry.

Recording coordination is initiated through a single GUI command. The software first stops the active synchronization output and arms the recording signal for the requested number of frames. It then brings the StreamPix acquisition window to the foreground and initiates optical recording, activates electrical recording in Open Ephys, and restarts the synchronization signal. This sequence reduces the number of independent manual actions required at the beginning of each acquisition.

Incoming serial data are monitored in a background thread. Sensor messages are decoded and sent to the appropriate display fields, while stimulation and controller-status messages update GUI indicators. Sensor plotting is handled by `sensor_plot_window.py` using Matplotlib with a TkAgg backend. The plotting window maintains rolling displays of tank temperature, perfusion pressure, inline temperature, and flow rate.

Experimental metadata are handled by `header_info.py`. Stored fields include experiment and specimen information, heart characteristics, optical-mapping parameters, electrical-acquisition settings, and operator notes. Metadata are written into the experiment log so that they remain associated with the corresponding dataset.

Directory monitoring is implemented using the Python `watchdog` package. The `directory_monitor.py` module records file creation, deletion, and renaming events within the acquisition directory. Manual annotations and received controller messages are stored with millisecond-resolution timestamps.

Configurable keyboard commands are managed through `hotkey_control.py`. Hotkey assignments are stored externally in JSON format and can therefore be changed without modifying the main GUI source code.

Single-channel current-mirror stimulator

The single-channel stimulator used in the small-heart experiments is shown in Supplementary Fig. S1. The output stage consists of a discrete PNP current mirror using one 2N5401 transistor in the reference branch and three parallel 2N5401 transistors in the output branch.

The 2N5401 was selected as a high-voltage PNP transistor compatible with the compliance voltage required for cardiac stimulation. Three devices were used in parallel at the output to increase current capability and distribute power dissipation between the transistors.

The reference current was adjusted using a 100-kΩ, 10-turn potentiometer in series with a 2.2-kΩ resistor. The multi-turn potentiometer provided fine manual adjustment of stimulation amplitude, while the fixed resistor limited the maximum current when the potentiometer approached its minimum resistance.

The approximate reference current is

$$I_{\mathrm{REF}} \approx \frac{V_{\mathrm{CC}} - V_{\mathrm{BE}}}{R_{\mathrm{POT}} + 2.2\ \mathrm{k\Omega}}. \tag{4}$$

For $V_{\mathrm{CC}} \approx 36$ V and $V_{\mathrm{BE}} \approx 0.7$ V, the reference branch provides an ideal range of approximately 0.35–16 mA. With three parallel output transistors,

$$I_{\mathrm{OUT}} \approx 3 I_{\mathrm{REF}}, \tag{5}$$

corresponding to an ideal range of approximately 1–48 mA. The experimentally used range was limited to approximately 1–45 mA because transistor mismatch, finite current gain, temperature, load impedance, and compliance voltage cause deviations from the ideal mirror relationship.

The stimulator was powered by four 9-V batteries connected in series, providing approximately 36 V and an effective compliance voltage of approximately 35 V. Battery operation provided a floating supply and reduced direct coupling of mains-frequency interference into the electrophysiological recording system.

The digital trigger was isolated using a PC817A optocoupler. The isolated signal drove a BC547A NPN transistor, which switched the current-mirror bias branch. This separated the digital control electronics from the stimulation circuit and reduced the formation of ground loops during simultaneous stimulation and electrical recording.

Stimulation was delivered through a bipolar pacing catheter with approximately 2-mm inter-electrode spacing.

Large-heart tank, transparent electrode PCB, and mechanical support

Additional dimensions of the large-heart whole-organ setup are shown in Supplementary Fig. S2.

The recording chamber was a transparent hexagonal acrylic tank with approximately 20 cm between opposing faces and a height of approximately 30 cm. Two removable transparent electrode PCBs were mounted on opposing tank faces to provide simultaneous electrical recording and optical access.

Each PCB contained 15 circular silver-plated electrodes arranged as a 5×3 array. The electrode diameter, inter-electrode distances, board outline, mounting points, and remaining mechanical dimensions are given directly in Supplementary Fig. S2A. Supplementary Fig. S2B shows the major tank dimensions.

The whole-heart support is shown in Supplementary Fig. S2C. The structure was designed to suspend a large heart inside the tank while allowing adjustment of height and orientation. Six ratchet-based positioning mechanisms were used during experiments to secure and adjust the support. The arrangement maintained access to the coronary cannulae while keeping the mapped cardiac surfaces clear of the transparent PCBs and optical paths.

Supplementary media

Supplementary Video S1. Synchronized optical and electrical recording from an ex vivo porcine heart. The video shows simultaneous optical activity from two camera views together with representative optical and electrical signals. Two optical signals are displayed for each camera view, with the corresponding sampling locations indicated by red markers on the optical images. Four simultaneously acquired electrical traces are shown below the optical signals. The red vertical cursors indicate the common time point represented by the displayed optical frames, illustrating temporal alignment between the optical and electrical recordings.

Supplementary figures

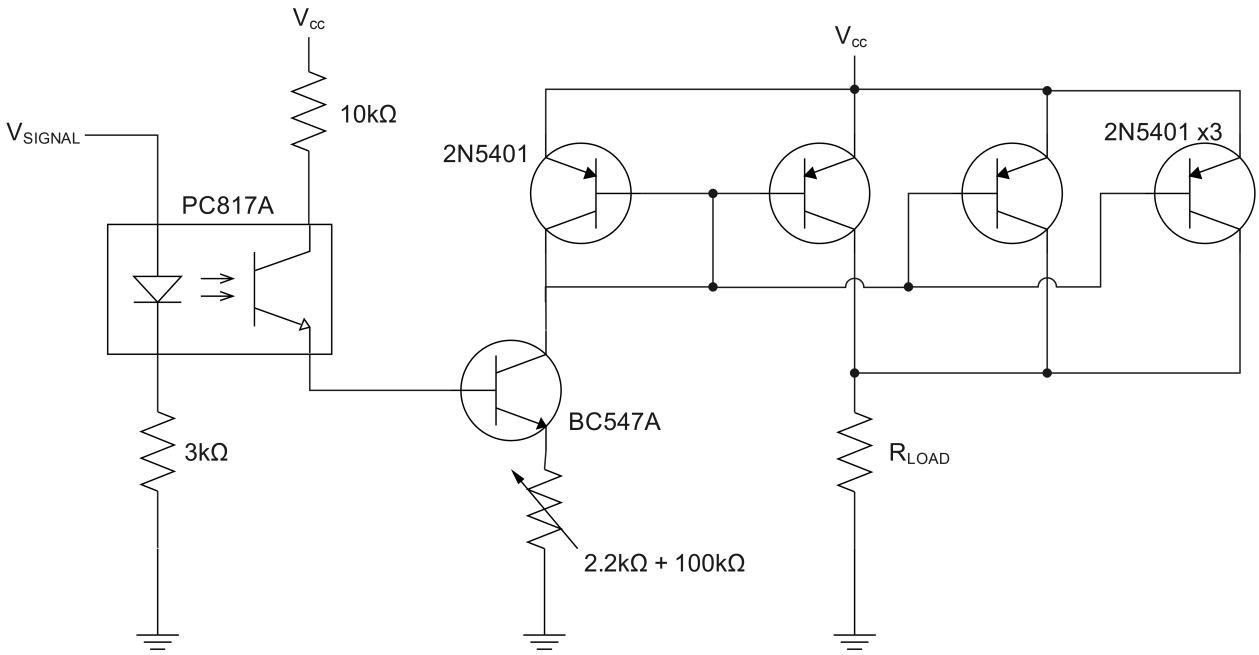


Figure 7. Supplementary Figure S1. Single-channel constant-current stimulator. Electrical schematic of the current-mirror stimulator used in the small-heart experiments. One 2N5401 PNP transistor forms the reference branch and three parallel 2N5401 transistors form the output branch. Current is adjusted using a 100-kΩ 10-turn potentiometer with a 2.2-kΩ series resistor. A PC817A optocoupler and BC547A switching stage provide isolated digital triggering. The circuit is powered by four series-connected 9-V batteries.

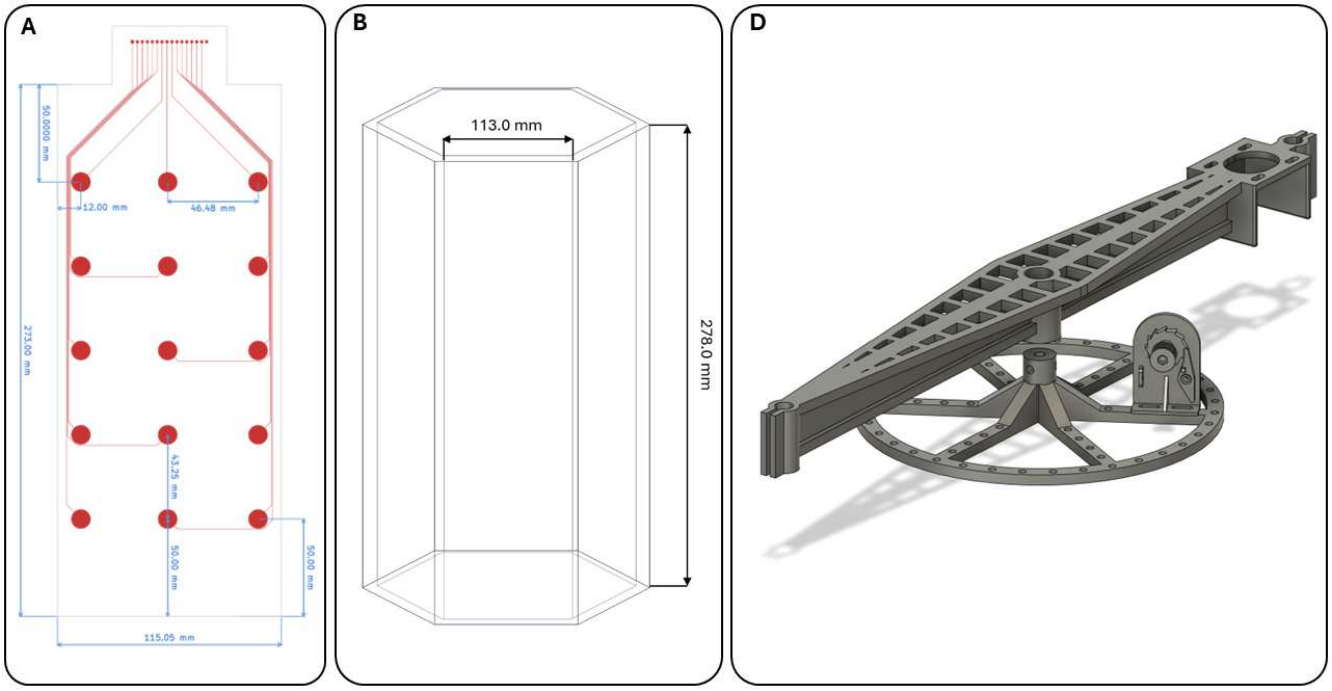


Figure 8. Supplementary Figure S2. Large-heart tank, electrode PCB, and mechanical support. **(A)** Detailed dimensions and electrode distribution of the transparent PCB used for large-heart bath-potential recording. **(B)** Principal dimensions of the hexagonal large-heart recording tank. **(C)** Three-dimensional render of the adjustable whole-heart support. Six ratchet mechanisms were used in the experimental implementation to position and stabilize the preparation.

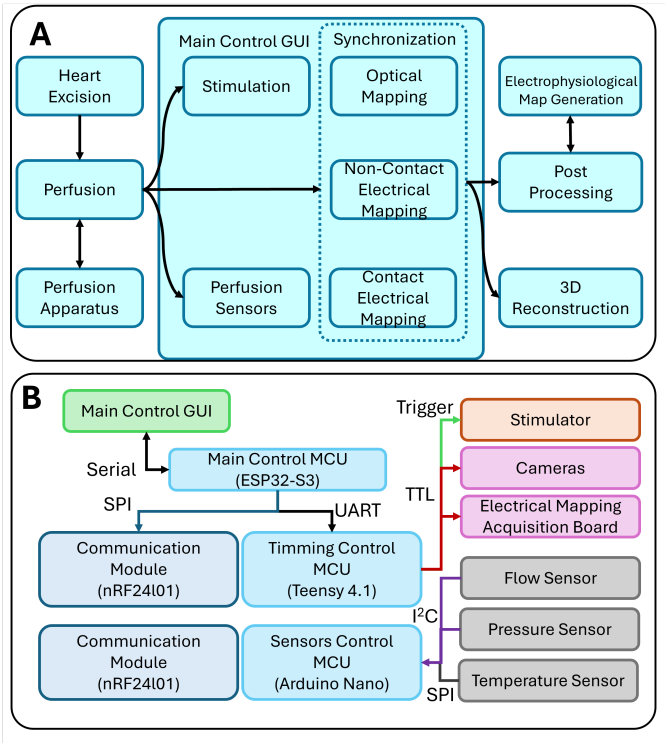


Figure 9. Experimental workflow and control architecture. **(A)** Experimental sequence from heart preparation and perfusion to synchronized optical, contact-electrical, and bath-electrical mapping, according to the experimental configuration. Physiological monitoring and electrical stimulation were integrated into the acquisition workflow. Following functional recordings, rotational imaging was performed for three-dimensional reconstruction, followed by signal processing and electrophysiological-map generation. **(B)** Control and monitoring architecture. A custom graphical user interface coordinated recording, synchronization, stimulation, sensor monitoring, directory monitoring, and experimental logging. The interface communicated with an ESP32-S3 gateway, while a Teensy 4.1 generated the synchronization signals to the optical and electrical acquisition systems and received measurements from distributed Arduino Nano sensor nodes through nRF24L01 wireless communication.

Supplementary Files

This is a list of supplementary files associated with this preprint. Click to download.

- TankPCBDimenssionsrender.png
- Currentmirror.png
- activationvideoporcine.mp4